Automatic Mesh Adaptation for Magnetic Pulse Forming Simulations

J.O. Garcia[1], J. R. Alves Z.[1,*], U. Ripert[1], J. Barlier[1], F. Bay[2]

[1] Transvalor S.A., E-Golf Park, 950 Avenue Roumanille, 06410 Biot, France.
[2] Mines Paris, PSL University, Centre for material forming (CEMEF), UMR CNRS, 06904 Sophia Antipolis, France
*Corresponding author. Email: jose.alves@transvalor.com

Abstract

Multiphysics coupling simulation for the electromagnetic modelling of pulse forming technology comes with several challenges: Large deformations with high strain rates, fast impact conditions, multiple phenomena with distinctive proper time scales, complex geometries, etc. In order to accurately represent the electromagnetic phenomena together with the thermomechanical effects in a reliable manner a key step is the ability to measure the numerical error intrinsic to the discretization scheme (typically within the finite element framework) and use of automatic mesh adaptation techniques. In this work, an a posteriori error estimator-based technique adapted to the electromagnetic phenomena is presented together with an anisotropic automatic mesh adaptation technique. These methods are rooted in the understanding of the underlying physical phenomena, bringing as consequence: ease of the modelling stage as numerical results are less dependent on initial mesh settings. Accelerated simulation times as computation resources are adapted automatically to increase accuracy where needed and decrease mesh density otherwise. All of this in a natively distributed-memory parallel framework which can be scaled for large problems within the simulation software FORGE®.

Keywords

Metal Forming, Finite element method (FEM)

1 Introduction

Magnetic Pulse Forming (MPF), a key high-speed forming process, enables deforming metallic components via pulsed Lorentz forces. Its contactless nature enables shaping and joining of materials often unfeasible with conventional methods (Psyk et al., 2011). MPF's ability to produce complex geometries and minimize spring back makes it especially appealing in automotive, aerospace, and electrical applications.

Simulating MPF can be computationally demanding due to the transient, nonlinear, and tightly coupled electromagnetic-mechanical interactions involved. High mesh resolution is essential near coils and workpiece surfaces, where electromagnetic fields vary sharply due to skin and proximity effects, while coarser meshes suffice in less active regions, such as surrounding air. This work presents a fully automatic anisotropic mesh adaptation strategy for finite element simulations of the MPF. By combining a posteriori error estimation with field-sensitive metric tensor construction, the method achieves high accuracy and reduced computational cost, adapting seamlessly to physical field variations and geometric complexity.

2 Error Estimators

A key component of the mesh adaptation strategy is the construction of an a posteriori error estimator that can guide local refinement or coarsening of the mesh. In this study, we adopt a residual minimization-based gradient recovery strategy to evaluate the discretization error of vector fields involved in electromagnetic simulations, such as the magnetic field or the electric field (Garcia et al., 2022). The methodology is established by formulating a global minimization problem:

$$min\left\|\vec{\mathrm{F}}_{\mathrm{P}_1} - \vec{\mathrm{F}}_{\mathrm{P}_0}\right\|^2 \tag{1}$$

Which in variational or weak form reads:

$$< \vec{\psi}, \vec{\mathrm{F}}_{\mathrm{P}_1} - \vec{\mathrm{F}}_{\mathrm{P}_0} >= 0 \tag{2}$$

where $\vec{\psi}$ represents the basis function of the Sobolev space $H(curl)$ used for electromagnetic fields. $\vec{\mathrm{F}}_{\mathrm{P}_1}$ represents an enriched (or recovered) representation of the base vector field $\vec{\mathrm{F}}_{\mathrm{P}_0}$.

Once the field has been recovered on the higher precision representation the error estimate is given by

$$\epsilon = \left\|\vec{\mathrm{X}}_{\mathrm{P}_1}(\mathrm{x}_\mathrm{G}) - \vec{\mathrm{X}}_{\mathrm{P}_0}(\mathrm{x}_\mathrm{G})\right\|_{\mathrm{L}^2(\Omega)} \tag{3}$$

where x_G represents the Gauss points coordinates of each element (e). Then, the error normalisation is given by

$$\|\epsilon\| = \frac{\epsilon_{L^2(\Omega_e)}}{\epsilon_{L^2(\Omega)}} \tag{4}$$

where $\epsilon_{L^2(\Omega_e)}$ and $\epsilon_{L^2(\Omega)}$ are the local and global error respectively. It is worth to point out that local defined error estimates generally do not take into consideration the directional effect of the anisotropy of the solution. However, a globally defined error estimator, as the one defined here, contains additional information about the solution, which allows to generate an anisotropic mesh adaptation approach.

3 Anisotropic Metric

The metric aiming to capture the anisotropic behaviour of the physical phenomenon is calculated from the Jacobian of a vector field describing it. This is achieved using the same Galerkin recovery or residual minimization recovery procedure applied in the error estimator. Let us consider a vector field F: $\mathbb{R}^3 \rightarrow \mathbb{R}^3$.
Depending on the geometrical nature of the field, two procedures can be envisioned:

3.1 Jacobian of a vector field

$$J(\vec{F}) = \vec{\nabla}(\vec{F})^T \vec{\nabla}(\vec{F}) \tag{5}$$

The procedure to calculate the metric from the Jacobian of F involves a sequence of smoothing and gradient calculation. Defining $\vec{F}_{P_1}$ at the element nodes, the gradient at the Gauss points is calculated as:

$$\vec{\nabla}\vec{F}_{P_0}(x_G) = \sum_{i=1}^{nodes} \vec{\nabla}\varphi_i \vec{F}_{P_1 i} \tag{6}$$

where φ represents the basis functions at the nodes. Then, the gradient at the element nodes is calculated by the recovery approach:

$$< \varphi, \vec{\nabla}\vec{F} - \vec{\nabla}\vec{F}_{P_0} >= 0 \tag{7}$$

3.2 Hessian from a scalar field

$$H(g) = \vec{\nabla}(\vec{\nabla}(g)) \tag{8}$$

The procedure to obtain the hessian from a scalar quantity is similar to the Jacobian procedure but the smoothing step has to be performed an additional time, as the gradient of the scalar field forms a first vector field which needs to be smoothed out.

3.3 Metric and normalization

The metric tensor forms the basis of the adaptive algorithm, providing the size, shape, and orientation of the new elements. The discretised metric is given as a function of the Jacobian tensor field at each node of the mesh: $M_i = M\big(J(x_i)\big)$. To build this metric, first,

the Jacobian is computed following the procedure above. Symmetry and positive definiteness are guaranteed by construction $\left(|\mathrm{T}|_i = \mathrm{T}_i^{\mathrm{T}}\mathrm{T}_i\right)$. The metric is then calculated by a filtering on the Jacobian matrix values, $\Lambda_\mathrm{i} = eigvals(J_i)$ and $\mathrm{R_i} = eigvecs(J_i)$. The eigenvalues link the required mesh size (h) along the eigenvector's directions with the error estimator. To avoid unrealistic metric specifications, such as infinite mesh sizes in an element, the eigenvalue is restrained applying an error tolerance (ϵ_0) and bounding the minimum (h_{min}) and maximum (h_{max}) mesh size, as follows:

$$\widetilde{\lambda_\mathrm{k}} = \min\left(\max\left(\frac{\sqrt{\lambda_\mathrm{k}}}{\epsilon_0}, \frac{1}{\mathrm{h}_{\mathrm{max}}^2}\right), \frac{1}{\mathrm{h}_{\mathrm{min}}^2}\right) \tag{9}$$

Finally, the metric is constructed as follows (for more details refer to):

$$\mathrm{M}_i = \mathrm{R}_i\widetilde{\Lambda}_i\mathrm{R}_i^{\mathrm{T}} \quad \text{with} \quad \widetilde{\Lambda}_i = \mathrm{diag}\left(\widetilde{\lambda_\mathrm{k}}\right) \tag{10}$$

4 Numerical Validation

Two study cases are used as demonstration examples. The first one is a well-established ring expansion semi-analytical case (Alves, 2016). The second one consists of a pancake-like configuration.

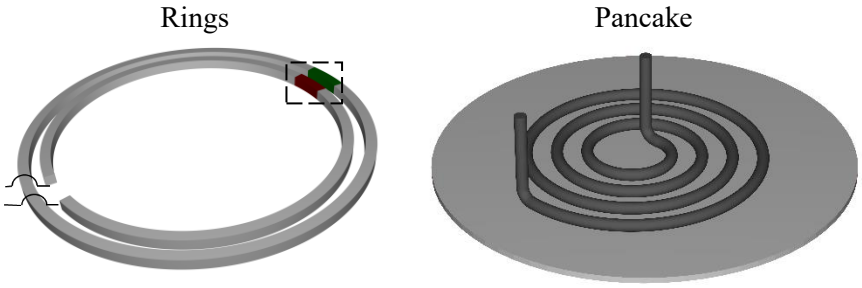

***Figure 1**: Magnetic Pulse Forming example cases: (left) Ring Expansion, (right) Bulging of a pancake configuration.*

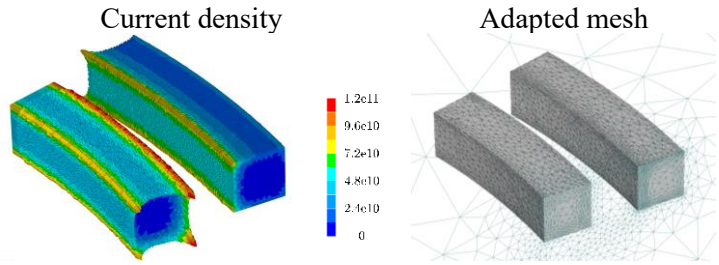

***Figure 2**: MPF case: Rings geometry, current density distribution [units=A/m^2] and adapted mesh*

Through the mesh adaptation procedure, the mesh is effectively refined and adjusted to capture the intricate electromagnetic phenomena. The conductive components, in particular, exhibit mesh adaptation in alignment with the anisotropy of the current density, effectively reducing the error evolution during computation, as illustrated in **Error!**

Reference source not found. while simultaneously reducing the overall computational time as seen in Table 1.

#Degrees of freedom		CPU time	
Initial mesh	Adapted mesh	Initial mesh	Adapted mesh
320.4 k	140 k	37 min	20 min

Table 1: *CPU times for the ring expansion case*

The objective of the investigation of the flat pancake configuration is to validate which metric tensor is able to capture the complexity of the magnetic field distribution in spite of the high aspect ratio of the geometry. A discharge pulsed signal with a natural frequency of 162kHz is used. The magnetic field ($\vec{H}$) is used to construct the metrics. Fig. 3 shows the comparison of the meshes and error distribution for both metrics and the initial mesh. It is observed that the Hessian metric achieves a smaller final error distribution than Jacobian. However, the difference between the degrees of freedom, shown in Table 2, is quite high in both of them, leading the metric Jacobian to require less degrees of freedom to achieve a mesh with an acceptable diminution of the error.

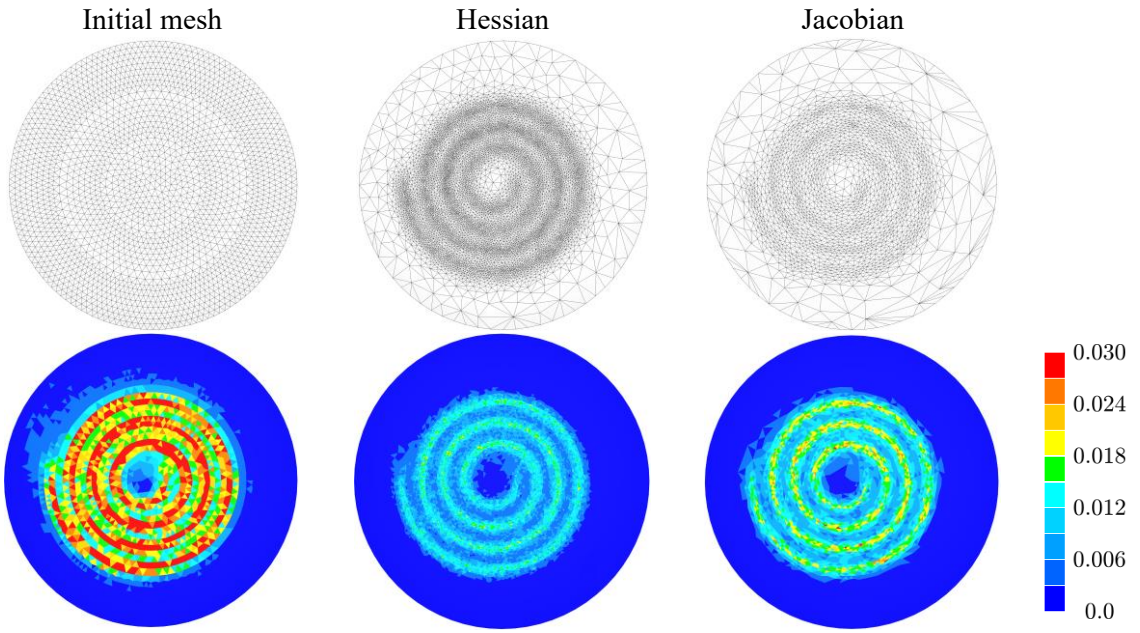

Figure 3*: Magnetic pulse forming mesh and error distribution (in percentage) results for the pancake configuration.*

Mesh	Initial	Hessian	Jacobian
Nodes	67805	79735	54292
elements	438928	465389	309727
Error [%]	$1.7x10^{-7}$	$0.9x10^{-7}$	$1.0x10^{-7}$

Table 2: *Mesh size and error estimator.*

Applying a cutting-plain view to the resulting mesh traversing the central plain of the circular geometry it can be seen in Fig. 4 how the methodology enables to automatically set fine mesh on the coils surface and within the workpiece near the coil. Both regions being the ones where the magnetic field reaches its peak and changes faster. The methodology will simultaneously keep a coarse mesh in regions of the air far-away such as to reduce the overall computational cost.

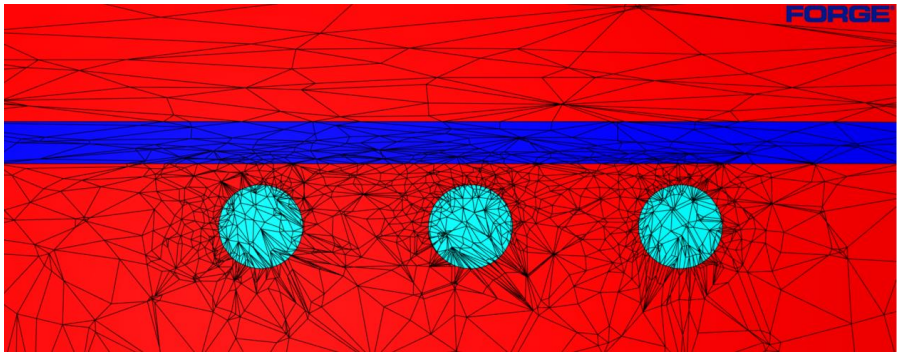

***Figure 4**: Cut-plain view of mesh density on the air, coil and workpiece.*

5 Conclusion

This work presents an efficient and robust mesh adaptation strategy that is both generic in formulation and efficient in computational terms to tackle the complexity arising from the magnetic pulse forming simulations. By employing a posteriori error estimation and a Jacobian-based metric tensor, the methodology enables to (a) capture high-gradient electromagnetic effects (e.g., skin effect) with fewer elements (b) align mesh elements with field directions, improving accuracy (c) reduce computational cost without sacrificing fidelity.

While both Hessian and Jacobian metrics are viable, the Jacobian-based approach shows superior anisotropy representation and error reduction for vector field-driven problems. Future work will explore the extending the method to other electromagnetic forming processes such as crimping and welding.

References

Alves, J., 2016. *Magnetic pulse forming processes: Computational modelling and experimental validation*. Université de recherche Paris Sciences et Lettres.

Garcia J., Alves, J., Barlier, J. and Bay, F., 2022. *A-Posteriori Error Estimator for Finite Element Simulation of Electromagnetic Material Processing*, *IEEE Trans Magn*, doi: 10.1109/TMAG.2022.3212597

Psyk, V., Risch, D., Kinsey, B.L., Tekkaya, A.E., Kleiner, M., 2011. *Electromagnetic forming – A review*. Journal of Materials Processing Technology 211 (5), pp. 787-829.